A comparison of the calculated and measured values of the pre-tilt angles are shown in Fig. 3a and b. The values of the pre-tilt angles were calculated using the equation described in the Methods section. For purposes of comparison with our experiments, we have adjusted the model calculations to match at one point of the pre-tilt versus ion-beam angle and pre-tilt versus ion-beam exposure time data. We note that the model predicts quite well the functional dependence of the pre-tilt angle with angle and time of exposure. A more detailed description of the model and its comparison with experiments, using both liquid-crystal and X-ray data, will be provided elsewhere (P.C., N.D.L., M.S., J.S. and J. Lüning, unpublished work). □

Methods

Optimization of hydrogen content in DLC films

The DLC films were deposited by plasma-enhanced chemical vapour deposition on glass substrates coated with a conducting indium tin oxide (ITO) film about 300 Å thick. Other substrates, such as Si and quartz, were also used for process comparison. The amorphous (a)-C : H films were deposited using C_2H_2/He and H_2 gas mixtures. Hydrogen was added to the process to increase film transmittance. The hydrogen content of the films was measured by forward recoil scattering. We used a process matrix to establish which process parameters yield higher hydrogen content and thus higher transmittance. In all of these experiments, the substrates were held at room temperature, which is important for cost considerations and also helped to obtain more transparent films than would a high-temperature process.

Ion-beam exposure

Ion beams were produced with a direct-current Kaufman-type ion source using a tungsten filament to supply electrons to the plasma and a plasma-bridge neutralizer to maintain charge neutrality. Argon was introduced into the ion source and plasma-bridge neutralizer using separate gas-flow controllers. The plasma-bridge neutralizer has the advantage of reduced substrate contamination as it is not physically immersed in the ion beam. In contrast, the commonly used tungsten-filament neutralizer, which is placed directly in the ion beam, is subject to sputtering by the energetic argon ions and neutrals impinging on it. Ions with energies in the range of 50–500 eV were extracted for the plasma within the ion source and accelerated toward the substrate. Ion current densities were measured using biased Faraday-cup probes to repel low-energy electrons introduced into the beam by the plasma-bridge neutralizer.

Substrates were mounted on a moving stage that was linearly scanned beneath the ion source. The tray speed was programmable, allowing different ion doses to be applied to the sample when using a fixed ion current density. The incident angle of the impinging ions could be varied by adjusting the angular position of the ion source relative to the substrate.

Calculation of the pre-tilt angle as a function of ion beam conditions

We quantify the model, described qualitatively in the text, by assuming that the destruction probability for a ring is proportional to the beam flux through it, and that we can neglect the effect of the destruction of other rings on that of a given ring. Let us assume a coordinate system with **x** normal to the surface and the ion beam incident in the x–y plane towards positive **z**, with angle of incidence α relative to the **z** axis. We define a vector **n** normal to a given ring, and denote the angle between **n** and the **z** axis as θ, and the azimuthal angle in the x–y plane as ϕ.

We denote by $\langle\theta\rangle$ the mean value of θ over the distribution of rings remaining on the surface at a time t, with beam exposure starting at $t = 0$. At $t = 0$, $\langle\theta\rangle = \pi/2$, because the beam distribution starts out isotropic. We take the product, denoted by W, of $\pi/2 - \langle\theta\rangle$ and the fraction of rings remaining on the surface at time t to be a measure of the pre-tilt angle; given the symmetry of the problem, we find that

$$W = \frac{1}{\pi}\int_0^{\pi}\left(\frac{\pi}{2} - \theta\right)\sin\theta\,\mathrm{d}\theta\int_0^{\frac{\pi}{2}}\exp(-pt\sin\alpha|\sin\alpha\sin\theta\cos\phi - \cos\alpha\cos\theta|)\,\mathrm{d}\phi$$

where p is proportional to the beam intensity, ring area, and destruction probability per unit time per unit beam flux through a ring. Using this equation, we have calculated the variation in the pre-tilt angle with the ion-beam dose and its angle of incidence. For details of the model, see P.C., N.D.L., M.S., J.S. and J. Lüning, unpublished work).

Received 30 November 2000; accepted 19 March 2001.

1. DeGennes, P. G. & Prost, J. *The Physics of Liquid Crystals* 161 (Clarendon, Oxford, 1993).
2. Stöhr, J. *et al.* Microscopic origin of liquid crystal alignment on buffed polymer surfaces. *Macromolecules* **31,** 1942–1946 (1998).
3. Stöhr, J. & Samant, M. G. Liquid crystal alignment by rubbed polymer surfaces: A microscopic bond orientation model. *J. Electron Spectrosc. Rel. Phenom.* **98–99,** 189–207 (1999).
4. Aoyama, H., Yamazaki, Y., Matsura, M., Mada, H. & Kobayashi, S. Alignment of liquid crystals on the stretched polymer films. *Mol. Cryst. Liq. Cryst.* **72,** 127–132 (1981).
5. Ikeno, Y. *et al.* Electrooptic bistability of a ferroelectric liquid crystal device using polyimide Langmuir–Blodgett orientation films. *Jpn J. Appl. Phys.* **27,** L475–L476 (1998).
6. Janning, J. L. Thin film surface orientation for liquid crystals. *Appl. Phys. Lett.* **21,** 173–174 (1972).
7. Schadt, M., Seiberle, H. & Schuster, A. Optical patterning of multi-domain liquid-crystal displays with wide viewing angles. *Nature* **381,** 212–215 (1996).
8. Berreman, D. W. Optics in stratified and anisotropic media: 4 × 4-matrix formulation. *J. Opt. Soc. Am.* **62,** 502–510 (1972).
9. Chaudhari, P., Lacey, J., Lien, S. A. & Speidell, J. L. Atomic beam alignment of liquid crystals. *Jpn J. Appl. Phys.* **37,** L55–L56 (1998).
10. Chaudhari, P., Graczyk, J. F., Henderson, D. & Steinhardt, P. Transformation between random network and dense random-packed models for amorphous solids. *Phil. Mag.* **31,** 727–732 (1975).

Acknowledgements

We thank T. Hashimoto for his encouragement and T. Ueki, H. Yamaguchi and M. Mitsuhashi for their sustained suport. P.C. thanks N. Okazaki for describing this technology to colleagues in Japan. G. Thompson photographed Figure 1.

Correspondence and requests for materials should be addressed to P.C. (e-mail: chaudha@us.ibm.com).

Size-dependent control of the binding of biotinylated proteins to streptavidin using a polymer shield

Zhongli Ding, Robin B. Fong, Cynthia J. Long, Patrick S. Stayton & Allan S. Hoffman

Department of Bioengineering, University of Washington, Seattle, Washington 98195, USA

Many medical and biotechnological processes rely on controlling and manipulating the molecular-recognition capabilities of proteins[1–4]. This can be achieved using small molecules capable of competing for protein binding or by changing environmental parameters that affect protein structure and hence binding. An alternative is provided by stimuli-responsive polymers that change reversibly from a water-soluble expanded coil to a water-insoluble collapsed globule upon small changes in temperature, pH or light intensity: when attached to proteins in the vicinity of their binding sites, they reversibly block and release small ligands[1,5–7]. Here we show how this approach can be extended to achieve size-selective binding of large, macromolecular ligands. We use the thermally responsive polymer poly(*N*,*N*-diethylacrylamide) (PDEAAm), and attach it to the protein streptavidin approximately 20 Å from the binding site for biotinylated proteins. Below the lower critical solution temperature of PDEAAm, the polymer is in its extended state and acts as a 'shield' to block the binding of large biotinylated proteins; above this temperature, it collapses and exposes the binding site, thereby allowing binding. We find that the degree of shielding depends on both the size of the biotinylated protein and the size of PDEAAm, suggesting that 'smart' polymer shields could be tailored to achieve a wide range of size-dependent ligand discrimination for use in affinity separations, biosensors and diagnostics technologies.

We have previously described the conjugation of stimuli-responsive polymers to genetically engineered sites near the binding site (or pocket) of streptavidin, yielding 'affinity switches' that control the binding and release of the small ligand biotin through small changes in environmental conditions[1,5–7]. The stimuli-responsive polymers reversibly cycle between an expanded coil and a collapsed globule in response to small changes in temperature, pH, or light, with a change in hydrodynamic radius of about three times[8]. In our previous work, the polymer was attached very close to one of

streptavidin's four biotin-binding pockets, and controlled the binding of biotin binding at this pocket.

Here we exploit the approximate C_{222} symmetry of the streptavidin tetramer, which gives rise to two distinct biotin-binding faces, with each binding face presenting two biotin-binding pockets separated by ~20 Å. This allows us to investigate the shielding activities of stimuli-responsive polymers attached at positions more distant from the biotin-binding site, as a function of the size of the ligand binding to streptavidin. Different molecular masses of the thermally responsive polymer, PDEAAm, were conjugated to a E51K/N118K streptavidin mutant and immobilized on magnetic microbeads (see Methods). This mutant was designed to enhance conjugation efficiency by localizing reactive primary amine groups near the biotin-binding pocket. Radiolabelled biotin-binding experiments showed that only one polymer could be conjugated per streptavidin-binding face.

The conjugate made from 12.8-kDa PDEAAm and E51K/N118K streptavidin (E51K/N118K–PDEAAm-12.8k) shielded the 20-Å-distant biotin-binding site against biotinylated proteins. Figure 1 shows that the amount of biotinylated bovine serum albumin (B-BSA) bound to this conjugate on the microbeads is temperature dependent, with low binding below 20 °C, followed by a sharp increase upon increase of temperature. Above 30 °C, the quantity of B-BSA bound to the conjugate is the same as that bound to the unconjugated E51K/N118K streptavidin. In the control, the binding of B-BSA to the unconjugated E51K/N118K streptavidin is high at all temperatures. The temperature dependence of the shielding effect thus closely corresponds to the phase transition behaviour of the polymer, which displays a lower critical solution temperature (LCST) of about 24 °C in the buffer solution.

The shielding activity of the streptavidin–PDEAAm-12.8k conjugate depends strongly on the size of the biotinylated protein target. A small (6.2 kDa) biotinylated protein, B-protein G, binds efficiently both above and below the LCST of PDEAAm (Fig. 1). B-protein G is not sterically shielded by the hydrated PDEAAm, and can access the nearby biotin-binding site whether the PDEAAm is extended or collapsed (Fig. 2). We also investigated a much larger target protein, biotinylated immunoglobulin-γ (B-IgG; 150 kDa) and found its binding to the conjugate was low over the entire temperature range. Due to the large size of B-IgG, its access to the binding site is effectively shielded even by the collapsed 12.8-kDa PDEAAm (Fig. 2).

Because of steric restrictions, each binding face of the unconjugated E51K/N118K streptavidin mutant can only bind one B-BSA. Thus, the low binding efficiency of B-BSA to E51K/N118K–PDEAAm-12.8k below the LCST of the conjugate (Fig. 1) arises because the extended, hydrated polymer coil obstructs access of B-BSA to the nearby binding pocket of streptavidin (Fig. 2). When the polymer is collapsed above the LCST, the binding site where the polymer is directly conjugated still remains shielded, while access to the nearby binding site at 20 Å distance is no longer obstructed, allowing binding of the B-BSA.

To confirm this shielding mechanism, we derivatized PDEAAm oligomers with biotin at one end, and showed that the biotinylated oligomer was able to associate with an average of only one binding site per binding face of the unconjugated E51K/N118K streptavidin mutant in solution. And when complexing one biotinylated 12.8-kDa PDEAAm per immobilized E51K/N118K streptavidin tetramer, the blocking of B-BSA as a function of temperature was similar to that seen with the immobilized conjugate (Fig. 3). This control experiment confirms that conjugation, as well as complexation, of a single smart polymer chain at a distance of about 20 Å to the nearby biotin-binding site can be used to reversibly shield and unshield that site.

The dependence of the shielding activity on the size of the biotinylated target proteins suggested that the size-selectivity of the polymer shields could be 'fine-tuned' by using polymers of different sizes. To test this, we prepared conjugates with PDEAAm oligomers of different molecular masses. At 10 °C, which is below the LCST of the PDEAAm, the amount of B-BSA bound to the

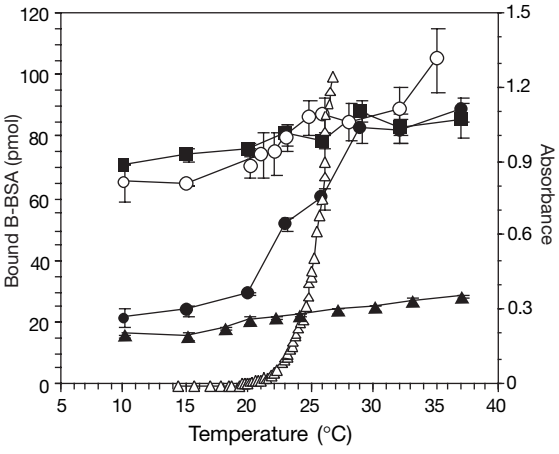

Figure 1 Shielding of biotinylated protein binding to E51K/N118K–PDEAAm conjugates. The binding of biotinylated BSA (B-BSA) to the E51K/N118K–PDEAAm-12.8k conjugate (filled circles) rises significantly as the temperature rises through the LCST (~23 °C), whereas the binding of B-BSA to unconjugated E51K/N118K streptavidin (filled squares) is efficient at all temperatures studied. The much smaller B-protein G binds to the E51K/N118K–PDEAAm-12.8k conjugate (open circles) efficiently over the whole temperature range investigated, while the binding of the large protein B-IgG to the E51K/N118K–PDEAAm-12.8k conjugate (filled triangles) is shielded over the entire temperature range. Under the binding conditions used (see Methods), the E51K/N118K–PDEAAm-12.8k conjugate has an LCST of ~23 °C (open triangles).

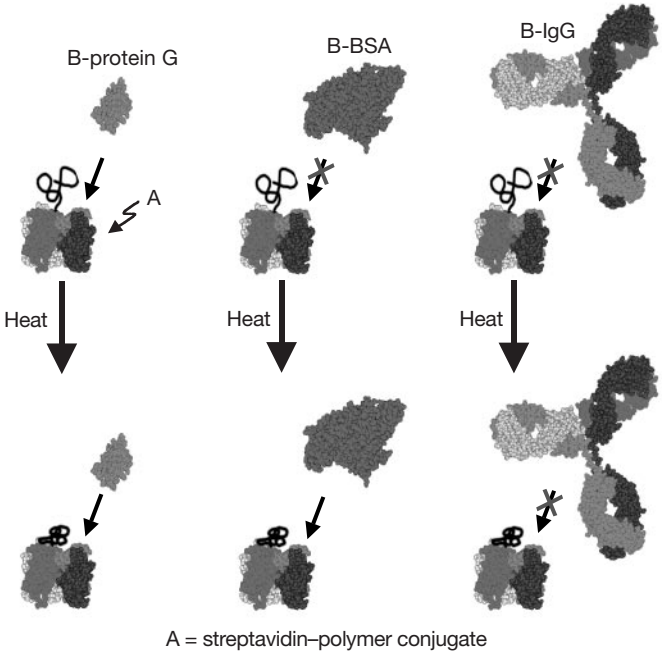

Figure 2 Schematic summary of the temperature sensitivity of the binding of biotinylated protein to streptavidin conjugates. The protein models were generated from Protein Data Bank files, with human albumin serving as a close analogue. The proteins are thus represented in proportion to their molecular sizes.

streptavidin–PDEAAm conjugates increases as the molecular mass of the conjugated polymer decreases (Figs 3, 4). This shows that the shielding activity can indeed be tuned by controlling the molecular mass of the conjugated polymer and supports the steric hindrance model, where smaller polymer chains provide less steric hindrance and allow greater access of biotinylated proteins to the adjacent binding site. As a further test of this model and of the size-selective shielding capabilities, we measured the ability of the streptavidin–PDEAAm-12.8-kDa conjugates to discriminate between B-protein G and B-BSA together in solution. The PDEAAm shield blocked B-BSA association, while allowing the B-protein G to bind to the same level as seen when it was the only protein in solution (data not shown). Thus, the conjugated smart polymer shields can also be used to discriminate amongst mixtures of proteins on the basis of size.

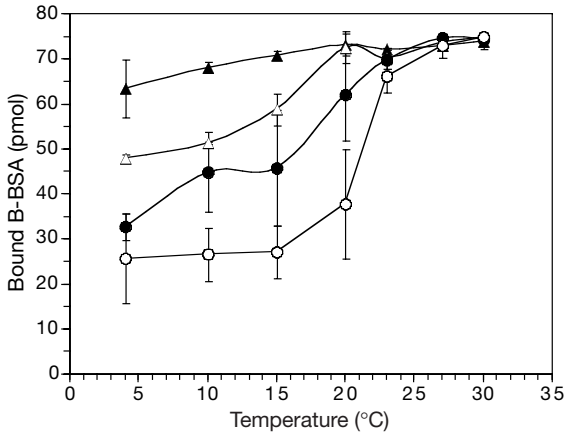

Figure 3 Shielding activity as a function of temperature and molecular mass of the PDEAAm polymer. Shown are the binding activities of B-BSA to immobilized E51K/N118K streptavidin that is either unconjugated, or forming an affinity-bound complex with biotinylated PDEAAm (B-PDEAAm) of different molecular masses. The graph shows the binding of B-BSA to E51K/N118K streptavidin (filled triangles) and complexes of E51K/N118K streptavidin and B-PDEAAm with molecular masses of 2.0 kDa (open triangles), 6.7 kDa (filled circles) and 12.8 kDa (open circles).

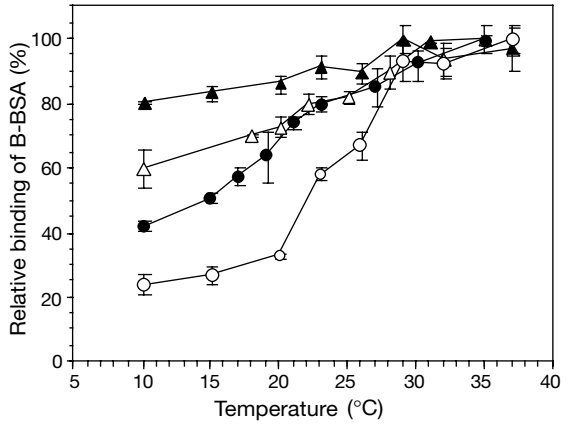

Figure 4 Effect of molecular mass of PDEAAm on the shielding efficiency. The graphs show the binding of B-BSA to E51K/N118K streptavidin (filled triangles) and covalent conjugates of E51K/N118K–PDEAAm with molecular masses of 2.0 kDa (open triangles), 6.7 kDa (filled circles) and 12.8 kDa (open circles). To compare the effect of the different-molecular-mass polymers on the shielding efficiency, we show relative binding of B-BSA, which is obtained by normalizing the amount of bound B-BSA to the maximum binding for each sample.

The small ligand biotin can access the binding pocket where the polymer is directly conjugated when the polymer is in the expanded state, allowing the collapse or expansion of the polymer to modulate association and/or dissociation[5–7]. However, the binding of the macromolecular biotinylated proteins is always blocked at the binding pocket where the polymer is conjugated. The biotinylated proteins thus provide a model system for developing the concept of the molecular shield, where the polymer is conjugated at a nearby but not directly adjacent site (in this case, approximately 20 Å away). The expanded polymer then becomes the active blocking state, because it can be engineered to be an appropriate size for sterically blocking access to the distant active site, whereas collapse unmasks the blocking activity in a size-dependent manner. This comparison is shown in Fig. 5.

The general approach should in principle be applicable to any protein active site, provided the polymer is conjugated at an appropriate distance from the active site so that its collapse unmasks that site. It should be possible to engineer the specificity and selectivity of these molecular shields, by matching the sizes of the polymer to those of the targets that undergo affinity binding. We expect that this approach to achieving size-selective shielding of protein active sites might find use in biotechnology applications. For example, control of the polymer coil size within or near the active site of a polymer–enzyme conjugate through temperature, pH or light signals, could favour the enzymatic transformation of smaller substrates, due to 'gating' (shielding) of large substrates. It might also be possible to use this approach to control access of pro-drugs to enzyme active sites, so that the active sites are obstructed while therapeutic enzymes travel to their target site, and opened on arrival. Similarly, it might be possible to efficiently separate mixtures of peptide and protein ligands on the basis of their binding affinity and size. Last, the reversible blocking and opening of immobilized protein arrays to target molecules such as peptides, DNA or photoactive molecules could open avenues to nanopatterning and information read/write technologies. □

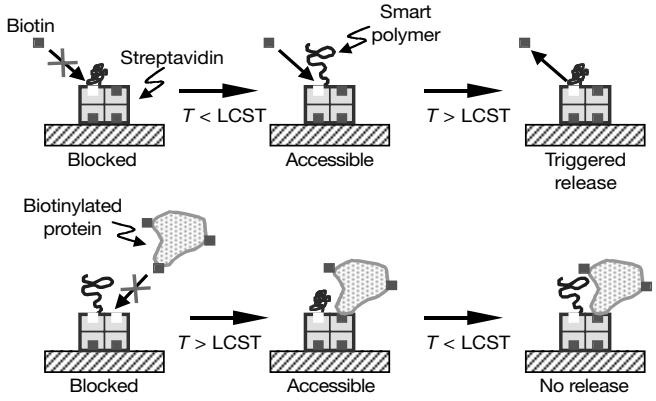

Figure 5 Schematic model of different shielding mechanisms. The model illustrates the shielding effects of a conjugated smart polymer on the binding of a small ligand (biotin) and a large macromolecular ligand (a biotinylated protein) to streptavidin. The polymer is in both cases conjugated to one binding site on the exposed face of an immobilized streptavidin molecule. (Only one polymer chain may be conjugated per binding face, due to steric hindrance). In the case of biotin association, the collapsed polymer blocks biotin access to the same site where the polymer is conjugated, but permits association at that site when the polymer is rehydrated and extended away from the site. In the case of the larger biotinylated protein, the conjugated polymer always blocks binding to the site where the polymer is conjugated, whether the polymer is collapsed or extended. The nearby binding site is exposed and accessible for binding of a biotinylated protein only when the polymer is collapsed, and provided the protein is small enough. Reversal of the stimulus can lead to release (depletion) of the biotin from the binding site where the polymer is conjugated[6,7] but there is no reversal expected for the biotinylated protein because the polymer is conjugated to the subunit 20 Å away from the binding site.

Methods

PDEAAm synthesis

PDEAAm was prepared by group transfer polymerization[9] to ensure a narrow molecular-mass distribution. Tetrabutylammonium acetate was used as the catalyst and 1-methoxyl-1-(trimethylsiloxy)-2-methyl-1-propene as the initiator. In the final stage of polymerization, a hydroxyl group was incorporated into one end of each polymer chain by adding a capping agent, 2-(trimethylsiloxy)ethyl methacrylate. The trimethylsiloxy group was subsequently removed by hydrolysis, to generate the –OH end group. The hydroxyl end group was subsequently derivatized to a vinyl sulphone group by reacting with divinyl sulphone[6,7]. The molecular mass and polydispersity of the polymer were determined in tetrahydrofuran, using gel permeation chromatography calibrated with polystyrene molecular-mass standards. All of the polymers have a molecular-mass polydispersity of less than 1.2.

Conjugation

Conjugation of PDEAAm to E51K/N118K streptavidin was performed at pH 9.5, 4 °C for 16 h. Three thermally induced precipitations of the conjugate were conducted to remove any unconjugated E51K/N118K streptavidin, which remained in the supernatant. Iminobiotin affinity chromatography was employed to separate the conjugate from the unreacted free polymer[10]. The purified streptavidin–PDEAAm conjugate was then immobilized on magnetic microbeads for the biotinylated-protein binding assays.

Binding assays

The conjugates and, as a control, the unconjugated E51K/N118K streptavidin were immobilized on magnetic microbeads and suspended in 100 mM sodium phosphate buffer, pH 8, containing 0.2 wt% of BSA. The suspensions were incubated in a 10 °C water bath for 1 h before addition of the biotinylated protein. They were mixed and then further incubated at 10 °C for 30 min to reach binding equilibrium. The magnetic beads were separated and the fluorescence intensities (excitation wavelength, 494 nm; emission wavelength, 520 nm) of the supernatant were measured versus control solutions without magnetic microbeads. The solutions were then incubated at a higher temperature and the same operations were repeated. One nmol of either E51K/N118K–PDEAAm conjugate or E51K/N118K was used for each assay.

Determination of LCST

The LCST of the E51K/N118K–PDEAAm-12.8k conjugate was determined in 100 mM sodium phosphate buffer, pH 8.0, containing 0.2 wt% of BSA, by measuring absorbance at 500 nm versus temperature. The LCST is defined as the temperature where the light absorbance is 10% of the maximum value.

Synthesis of biotinylated PDEAAm

A primary amino group at the end of the PDEAAm chain was reacted with sulph-NHS-LC-biotin (from Pierce). B-PDEAAm was then complexed to E51K/N118K streptavidin, which was immobilized on magnetic beads via the interaction of biotin and streptavidin.

Received 29 December 2000; accepted 12 February 2001.

1. Fong, R. B., Ding, Z., Long, C. J., Hoffman, A. S. & Stayton, P. S. Thermoprecipitation of streptavidin via oligonucleotide-mediated self-assembly with poly(N-isopropylacrylamide). *Bioconj. Chem.* **10,** 720–725 (1999).
2. Wilchek, M. & Bayer, E. A. *Avidin–Biotin Technology* (Academic, New York, 1990)
3. Schlosser, M., Hahmann, J., Ziegler, B., Augstein, P. & Ziegler, M. Sensitive monoclonal antibody-based sandwich ELISA for determination of the diabetes-associated autoantigen glutamic acid decarboxylase GAD65. *J. Immunoass.* **18,** 289–307 (1997).
4. Bloch, B. Biotinylated probes for in situ hybridization histochemistry: Use for mRNA detection. *J. Histochem. Cytochem.* **41,** 1751–1754 (1993).
5. Stayton, P. S. *et al.* Control of protein-ligand recognition using a stimuli-responsive polymer. *Nature* **378,** 472–474 (1995).
6. Bulmus, V., Ding, Z., Long, C. J., Stayton, P. S. & Hoffman, A. S. Design, synthesis and site-specific conjugation of a pH- and temperature-sensitive polymer to streptavidin for pH-controlled binding and triggered release of biotin. *Bioconj. Chem.* **11,** 78–83 (1999).
7. Ding, Z. *et al.* Temperature control of biotin binding and release with a streptavidin-poly(N-isopropylacrylamide) site-specific conjugate. *Bioconj. Chem.* **10,** 395–400 (1999).
8. Wu, C. & Wang, X. H. Globule-to-coil transition of a single homopolymer chain in solution. *Phys. Rev. Lett.* **80,** 4092–4094 (1998).
9. Sogah, D. Y., Hertler, W. R., Webster, O. W. & Cohen, G. M. Group transfer polymerization. Polymerization of acrylic monomers. *Macromolecules* **20,** 1473–1488 (1987).
10. Hofmann, K., Wood, S. A., Brinton, C. C., Montibeller, J. A. & Finn, F. M. Iminobiotin affinity columns and their application to retrieval of streptavidin. *Proc. Natl Acad. Sci. USA* **77,** 4666–4668 (1980).

Acknowledgements

We thank R. Clark for providing protein G, and N. Murthy for help with PDEAAm synthesis. This work was supported by the National Institutes of Health.

Correspondence and requests for materials should be addressed to A.S.H. (hoffman@u.washington.edu) or P.S.S. (stayton@u.washington.edu).

Evolution of Asian monsoons and phased uplift of the Himalaya–Tibetan plateau since Late Miocene times

An Zhisheng*, John E. Kutzbach†, Warren L. Prell‡ & Stephen C. Porter§

** State Key Laboratory of Loess and Quaternary Geology, Institute of Earth Environment, Chinese Academy of Sciences, Box 17, Xi'an 710054, China*
† Center for Climatic Research, Institute for Environmental Studies, University of Wisconsin-Madison, 1225 W. Dayton Street, Madison, Wisconsin 53706, USA
‡ Geological Sciences, Box 1846, Brown University, Providence, Rhode Island 02912-1846, USA
§ Quaternary Research Center, Box 351310, University of Washington, Seattle, Washington 98195, USA

The climates of Asia are affected significantly by the extent and height of the Himalayan mountains and the Tibetan plateau[1–4]. Uplift of this region began about 50 Myr ago, and further significant increases in altitude of the Tibetan plateau are thought to have occurred about 10–8 Myr ago[4,5], or more recently. However, the climatic consequences of this uplift remain unclear. Here we use records of aeolian sediments from China[6,7] and marine sediments from the Indian[8–10] and North Pacific oceans[11] to identify three stages of evolution of Asian climates: first, enhanced aridity in the Asian interior and onset of the Indian and east Asian monsoons, about 9–8 Myr ago; next, continued intensification of the east Asian summer and winter monsoons, together with increased dust transport to the North Pacific Ocean[11], about 3.6–2.6 Myr ago; and last, increased variability and possible weakening of the Indian and east Asian summer monsoons and continued strengthening of the east Asian winter monsoon since about 2.6 Myr ago. The results of a numerical climate-model experiment, using idealized stepwise increases of mountain–plateau elevation, support the argument that the stages in evolution of Asian monsoons are linked to phases of Himalaya–Tibetan plateau uplift and to Northern Hemisphere glaciation.

Continuous sedimentary records of Asian climate are found in China and in marine cores from the Indian and North Pacific oceans (Fig. 1). The planktonic foraminifer *Globigerina bulloides* and upwelling radiolaria from ODP site 722 (Fig. 2) are indices of coastal upwelling in the Arabian Sea and thus of southwesterly wind strength during the Indian summer monsoon[8,10]. Although carbonate dissolution (often associated with high productivity) reduces the magnitude of the *G. bulloides* index at certain times (Fig. 2), the composite radiolarian and *G. bulloides* records show strengthening of upwelling about 9–8 Myr ago and relatively continuous upwelling thereafter. Magnetic susceptibility flux from ODP site 758 (ref. 9), representing sea-level-mediated fluvial transport from the Ganges and other river systems draining the southern side of the Himalayan–Tibetan orogen, increases about 9 Myr ago. Significantly, new basal dates from the aeolian 'Red Clay' sediments on the Chinese Loess plateau (Figs 1, 2) indicate onset of aeolian dust accumulation at about 7.6 Myr ago at Zhaojiachuan (35° 53′ N, 107° 58′ E), 8.0 Myr ago at Chaona (35° 06′ N, 107° 12′ E), and as early as 8.3 Myr ago at Jiaxian (38° 16′ N, 110° 5′ E) (Fang, X.M. and Qiang, X.K., personal communication). Records from North Pacific ODP sites 885 and 886, which accumulated wind-blown dust from Asia, show a major dust peak about 8–7 Myr ago[11]. The change in oxygen isotope composition of soil carbonates in Pakistan about 9–8 Myr ago[12] (Fig. 2), inferred changes in vegetation from C_3 (forests) to C_4 (grasses) in Pakistan beginning about 8 Myr ago[13], and a change from mixed needle-leaf and broad-leaf forests to grassland vegetation along the northeastern margin of the Tibetan plateau about 8.5 Myr ago[14], all imply increasing seasonality by about 8 Myr